

Rectified SpaAttn: Revisiting Attention Sparsity for Efficient Video Generation

Xuewen Liu^{1,2}, Zhikai Li^{1*}, Jing Zhang^{1,2}, Mengjuan Chen¹, Qingyi Gu^{1*}

¹Institute of Automation, Chinese Academy of Sciences

²School of Artificial Intelligence, University of Chinese Academy of Sciences

{liuxuewen2023, zhikai.li, qingyi.gu}@ia.ac.cn

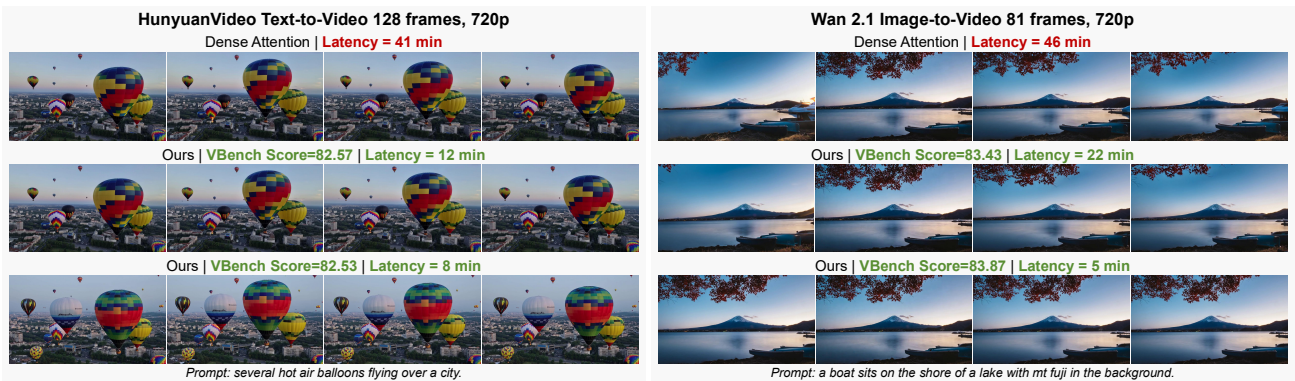


Figure 1. Rectified SpaAttn achieves significant speedup while maintaining high quality, making video generation more efficient.

Abstract

Diffusion Transformers dominate video generation, but the quadratic complexity of attention computation introduces substantial latency, hindering real-world applications. Attention sparsity reduces computational costs by focusing on critical tokens while ignoring non-critical tokens. However, existing methods suffer from severe performance degradation, especially under high sparsity. In this paper, we revisit attention sparsity and show, through theoretical analysis, that existing methods induce systematic biases in attention allocation: (1) excessive focus on critical tokens amplifies their attention weights; (2) complete neglect of non-critical tokens causes the loss of relevant attention weights. To address these issues, we propose Rectified SpaAttn, which rectifies sparse attention allocation with implicit full attention reference, thereby enhancing the alignment between sparse and full attention maps. Specifically, we implicitly capture the full-attention distribution of critical and non-critical tokens by pooled query-key interactions, without explicit computation, which is then used to rectify sparse attention allocation: (1) for critical tokens, we show that

their bias is proportional to the sparse attention weights, with the ratio governed by the amplified weights. Accordingly, we propose Isolated-Pooling Attention Reallocation, which calculates accurate rectification factors by reallocating multimodal pooled weights. (2) for non-critical tokens, recovering attention weights from the pooled query-key yields attention gains but also introduces pooling errors. Therefore, we propose Gain-Aware Pooling Rectification, which ensures that the rectified gain consistently surpasses the induced error. Moreover, we customize and integrate the Rectified SpaAttn kernel using Triton, achieving up to 3.33 \times and 2.08 \times speedups on HunyuanVideo and Wan 2.1, respectively, while maintaining high generation quality. We release Rectified SpaAttn as open-source at <https://github.com/BienLuky/Rectified-SpaAttn>.

1. Introduction

Diffusion Transformers (DiTs) [20] have achieved remarkable success in video generation tasks [10, 25]. However, the inference efficiency of DiTs remains a major bottleneck, primarily due to the quadratic complexity of attention computation [24]. As an example, generating a 128-frame 720p video with HunyuanVideo [10] on an NVIDIA H100 PCIe requires approximately 41 minutes end-to-end, where atten-

*Corresponding author: {zhikai.li, qingyi.gu}@ia.ac.cn.

tion mechanisms dominate 32 minutes of the latency even with FlashAttention [4] optimization.

To reduce the computational complexity of attention mechanisms, attention sparsity [23, 29] restricts each query token to interact with only a small subset of critical key-value tokens, thereby omitting most non-critical computations. Typically, the importance of a token is determined by its full-attention weight: tokens with larger weights are regarded as critical, while those with smaller weights are considered non-critical. To support block-wise computation optimizations such as FlashAttention [4], this identification is performed at the block level. In addition, since visual tokens within a block exhibit strong homogeneity, existing methods [27, 28, 33, 34] evaluate visual block importance using pooled attention weights derived from uniformly pooled query-key interactions. It significantly reduces the overhead of evaluation. After evaluation, sparse mask [34] identifies critical tokens, guiding the subsequent sparse computation.

Although existing methods [12, 22, 27, 32, 34] remain effective at low sparsity ratios, their performance degrades drastically at higher levels. For example, The Vision Reward [31] of Jenga [34] drops to 0.0585 under 90% sparsity ratio. To investigate the underlying cause, we revisit attention sparsity and reveal that existing methods induce systematic biases in attention allocation, as shown in Fig. 2.

(1) Allocation bias of critical tokens: Since attention sparsity involves only critical tokens in the softmax normalization, their attention weights are amplified relative to full attention. For instance, a critical token with a weight of 0.8 under full attention may rise to 1.0 under sparse attention. As a result, the attention outputs of critical tokens deviate from those of full attention, and the bias becomes more pronounced as the sparsity ratio increases.

(2) Allocation bias of non-critical tokens: Attention sparsity completely omits computations for non-critical tokens, causing their attention weights to be discarded. For instance, non-critical tokens with attention weights of 0.2 under full attention will become 0.0 under sparse attention. This results in information loss compared to full attention, and the bias also further increases as sparsity ratio grows.

To address the above issues, we propose **Rectified SpaAttn**, a training-free framework that rectifies sparse attention allocation to enhance the alignment between sparse and full attention maps. Our method is motivated by a key observation: *Pooled attention weights derived from uniformly pooled query-key interactions can implicitly capture the full-attention distribution of critical and non-critical tokens.* (as shown in Fig. 3b). Therefore, we leverage them as implicit full attention to guide the rectification:

(1) For critical tokens, we demonstrate that their bias is proportional to the attention weights, with the ratio determined by the amplified weights. Thus, the bias can be rec-



Figure 2. Sparsity results in systematic attention biases.

tified by the full-attention weights. Based on this, we calculate rectified factor using the pooled attention weights, avoiding the costly explicit full attention. However, since text tokens lack intra-block homogeneity, directly pooling them causes large errors. To address this, we propose Isolated-Pooling Attention Reallocation (IPAR), which isolates text tokens during pooling and reallocates weights afterward to obtain accurate pooled attention weights.

(2) For non-critical tokens, we recover attention weights using the pooled attention map. However, since the rectification relies on block-level pooled weights to approximate token-level weights, it yields attention gains but also introduce pooling errors. To this end, we propose Gain-Aware Pooling Rectification (GAPR), which estimates the attention gains and pooling errors, and performs rectification only when the gain surpasses the error, thereby ensuring stable performance improvement.

We evaluate our method on representative generative models, including HunyuanVideo-T2V [10], Wan2.1-T2V/I2V [25], and Flux.1-dev [11]. Results demonstrate that Rectified SpaAttn outperforms existing methods [12, 22, 27, 32, 34] across various sparsity ratios, particularly under higher sparsity. Specifically, Rectified SpaAttn achieves up to a 3.33× end-to-end speedup under 90% sparsity ratio, while maintaining high visual quality with a VBench Score [7] of up to 82.57 on HunyuanVideo. By further combining with caching techniques [14], our method achieves 5.24×, 8.97×, and 4.15× speedups on HunyuanVideo-T2V, Wan2.1-I2V, and Flux.1-dev, respectively. Overall, our key contributions are as follows:

- We revisit attention sparsity, and reveal the limitations of existing methods as systematic biases in attention allocation: excessive focus on critical tokens amplifies their attention weights, while complete neglect of non-critical tokens causes the loss of relevant attention weights.
- We propose Rectified SpaAttn, which leverages implicit full attention to guide the rectification of allocation biases, aligning sparse attention with its full counterpart. We introduce IPAR and GAPR to ensure accurate rectification for critical and non-critical tokens, respectively.
- Rectified SpaAttn pushes the sparsity limit while preserving high generation quality. We further optimize it with Triton and package it as a plug-and-play attention module for efficient and scalable deployment.

2. Related Work

Efficient Video Generation. The high inference cost of video generation [13] remains a major bottleneck, severely constraining their applicability in real-world scenarios. To reduce computation, timestep compression [5] shorten the trajectory by rectifying generation objectives. Model compression include model pruning [2] to reduce parameter scale, model quantization [15, 17] to lower parameter bit-width, and model distillation [19] to construct lightweight models. Additionally, model caching [14, 16, 18] leverage the high similarity between timesteps, improving efficiency through feature reuse. Although these methods have achieved remarkable success, they are mostly applied to low-resolution image or short video generation. With the growing demand for long video generation, models are required to process 50K~200K tokens. The quadratic complexity of attention thus causes a drastic rise in computation, becoming the main bottleneck of inference.

Attention Sparsity. Previous studies [29, 35] have shown that attention in transformers exhibit nature sparsity. Building on this, several works [8, 23] retain only the interactions between query tokens and critical key-value tokens to reduce attention computation, known as attention sparsity. SVG [27] explores it for DiTs by designing spatial and temporal sparse mask. AdaSpa [28] dynamically evaluates token importance and adaptively constructs blockified sparse mask. STA [33] and GRAT [22] leverage the locality of attention by maintaining fixed tiled attention windows. RadialAttention [12] exploits the decay of attention and design a radial sparse mask. SVG2 [32] applies k-means clustering to reorder tokens and defines block-wise sparse masks. Jenga [34] reorders token sequences using space-filling curves to enhance intra-block coherence. Despite notable progress, most methods reach only around 75% sparsity. At higher sparsity, the performance of them degrades sharply, making it difficult to balance speedup and quality.

3. Motivation

3.1. Systematic Biases in Attention Allocation

In DiTs, attention integrates video and text tokens into a unified sequence [10]. Specifically, video queries $Q_v \in \mathbb{R}^{T_v \times d}$ handle video-video and video-text attention, while text queries $Q_t \in \mathbb{R}^{T_t \times d}$ handle text-video and text-text attention, where T_v and T_t denote the token lengths of video and text, respectively, and d is the feature dimension. Since $T_v \gg T_t$ and video tokens exhibit redundancy, existing methods [12, 22, 27, 28, 32–34] apply sparsity only to Q_v while retaining full attention for Q_t . For simplicity, we use Q to denote Q_v and focus on its attention. Additionally, to reduce frequent memory access, attention computation is typically performed in block level[4], where consecutive Q

and KV are aggregated into a block, denoted as:

$$Q = [Q_1, Q_2, \dots, Q_N], Q_n \in \mathbb{R}^{B^q \times d} \quad (1)$$

$$K = [K_1, K_2, \dots, K_M], K_m \in \mathbb{R}^{B^k \times d} \quad (2)$$

$$V = [V_1, V_2, \dots, V_M], V_m \in \mathbb{R}^{B^k \times d} \quad (3)$$

Here, B^q and B^k denotes the block sizes of query and key, respectively. In our experiments, we set $B = B^q = B^k = 128$. $N = \frac{T_v}{B}$ and $M = \frac{T_v + T_t}{B}$ represent the number of blocks for Q and KV , respectively. The full attention weight for the Q_n can be formulated as:

$$S_n = \frac{Q_n K^T}{\sqrt{d}}, A_n = \text{softmax}(S_n) \quad (4)$$

Attention sparsity reduces computational cost by limiting the interaction number of KV tokens. To align with block-wise computation, sparsity is also applied at the block level: if a block is identified as critical, all KV tokens within it are preserved; otherwise, the entire block is discarded, as illustrated in Fig. 4. Existing methods [12, 27, 34] evaluate the importance of block to generate sparse masks $\widehat{M} \in \{0, 1\}^{N \times M}$, where $\widehat{M}_{n,m} = 1$ indicates that Q_n is permitted to interact with K_m and V_m , and $\widehat{M}_{n,m} = 0$ otherwise. Therefore, the sparse attention weight for the Q_n is formulated as:

$$S_n^{spa} = \frac{Q_n K^T \odot \widehat{M}_n}{\sqrt{d}}, A_n^{spa} = \text{softmax}(S_n^{spa}) \quad (5)$$

According to Eq. 4 and Eq. 5, our theoretical analysis reveals that attention sparsity induces systematic allocation biases, leading to large output errors, as shown in Fig. 3a.

(1) For critical tokens, assuming the K_{m-1} , their attention weights for Q_n in full and sparse attention are donates as:

$$A_{n,m-1} = \frac{\exp(S_{n,m-1})}{\sum_{m=1}^M \exp(S_{n,m})} \quad (6)$$

$$A_{n,m-1}^{spa} = \frac{\exp(S_{n,m-1})}{\sum_{m=1}^M \exp(S_{n,m}) \cdot \widehat{M}_{n,m}}$$

As can be seen, due to the reduced number of elements involved in softmax normalization, $|\widehat{M}_n| < M$, $|\widehat{M}_n|$ denoting the number of preserved K blocks for Q_n , their attention weights are amplified compared to those in full attention, $A_{n,m-1}^{spa} > A_{n,m-1}$. This is regarded as an excessive focus on critical tokens, which introduces attention bias.

(2) For non-critical tokens, assuming the K_m , their attention weights for Q_n are formulated as:

$$A_{n,m} = \frac{\exp(S_{n,m})}{\sum_{m=1}^M \exp(S_{n,m})} \quad (7)$$

$$A_{n,m}^{spa} = \frac{0}{\sum_{m=1}^M \exp(S_{n,m}) \cdot \widehat{M}_{n,m}}$$

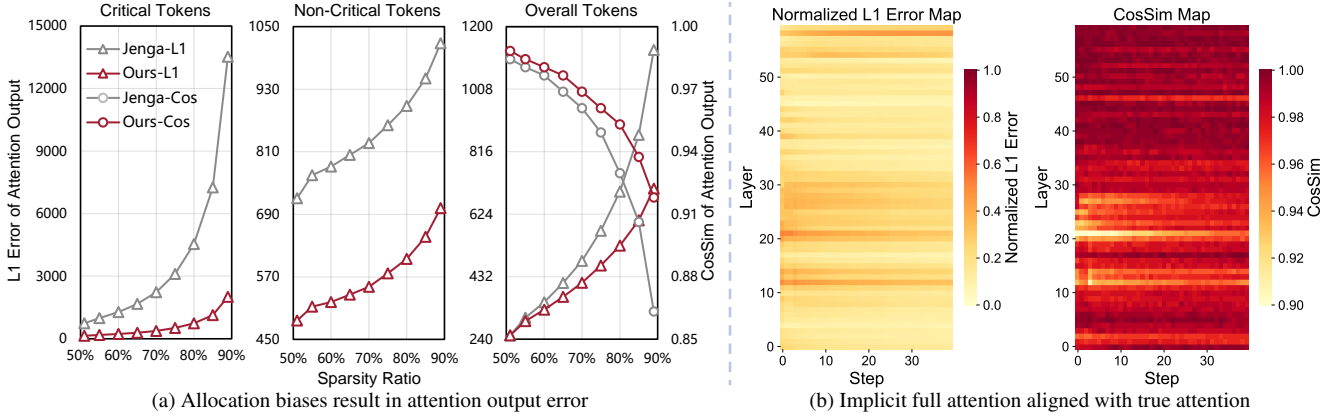


Figure 3. **Motivation.** (a) Attention sparsity introduces allocation biases that cause large output errors, which intensify as sparsity increases. (b) Implicit full attention obtained by IPAR exhibits strong alignment with the true full attention in both magnitude and distribution, as evidenced by lower normalized L1 error and higher cosine similarity across timesteps and layers under 80% sparsity. The normalized L1 error is computed as the L1 difference normalized by the magnitude of the true attention. Data come from HunyuanVideo.

Due to the complete omission of computation, their attention weights are discarded compared to those in full attention, $\mathbf{A}_{n,m}^{spa} = 0$. This results in the loss of their attention, thereby also introducing attention bias.

Clearly, these biases intensify as the sparsity increases. Although existing methods strive to design sparse masks, the performance degrades significantly at high sparsity.

3.2. Implicit Full Attention

Based on the analysis in Sec 3.1, we explore *how to rectify the systematic biases to enhance the alignment between sparse and full attention maps*. Evidently, the rectification can be achieved by leveraging the full attention weights. However, explicit full attention incurs significant computational overhead, which contradicts the purpose of attention sparsity and undermines its acceleration benefits.

Previous methods [8, 34] uniformly pooled the visual $\mathbf{Q}\mathbf{K}_v$ to compute relative pooled attention weights $\mathbf{A}_r^{pool} \in \mathbb{R}^{N \times N}$, which are used to evaluate the importance of visual blocks. In contrast, we observe that the pooled attention weights $\mathbf{A}^{pool} \in \mathbb{R}^{N \times M}$, derived from uniformly pooled the complete $\mathbf{Q}\mathbf{K}$ interactions, inherently possess the capacity to implicitly capture the full-attention distribution of critical and non-critical tokens. Specifically, they exhibit strong consistency with full-attention weights in both magnitude and distribution, as shown in Fig. 3b. Therefore, it can not only evaluate block importance but also guide bias rectification. The formulation is expressed as:

$$\begin{aligned}
 \mathbf{Q}_n^{pool} &= \frac{1}{B} \sum_{i \in B_n^q} Q_i \\
 \mathbf{K}^{pool} &= \left[\frac{1}{B} \sum_{j \in B_1^k} K_j, \frac{1}{B} \sum_{j \in B_2^k} K_j, \dots, \frac{1}{B} \sum_{j \in B_M^k} K_j \right] \quad (8) \\
 \mathbf{S}_n^{pool} &= \frac{\mathbf{Q}_n^{pool} \mathbf{K}^{pool T}}{\sqrt{d}}, \quad \mathbf{A}_n^{pool} = \text{softmax}(\mathbf{S}_n^{pool})
 \end{aligned}$$

where B_n^q and B_m^k represent the index sets within query and key blocks, respectively. \mathbf{Q}_n^{pool} and \mathbf{K}^{pool} denote the uniformly pooled representations of \mathbf{Q}_n and \mathbf{K} . Note that directly pooling text tokens in \mathbf{K} leads to information loss, which we address in Sec. 4.1. As the computation is performed on the pooled $\mathbf{Q}\mathbf{K}$ blocks, the computational complexity is significantly reduced. Moreover, since $T_v \gg T_t$, it introduces only a negligible overhead compared with \mathbf{A}_r^{pool} . Given its advantages in accuracy and efficiency, we regard the pooled attention weights as implicit full attention to guide the rectification of systematic biases.

4. Rectified SpaAttn

4.1. Rectifying the Bias of Critical Tokens

For critical tokens, assuming the \mathbf{K}_m , their sparse attention weights satisfy $\mathbf{A}_{n,m}^{spa} > \mathbf{A}_{n,m}$ as analyzed in Sec 3.1, indicating an attention amplification bias. To rectify this bias, we aim to align $\mathbf{A}_{n,m}^{spa}$ with $\mathbf{A}_{n,m}$. According to Eq. 6, we find that the sparse attention weights are proportional to the full-attention weights. Therefore, we introduce a rectified factor $\mathbf{R} \in \mathbb{R}^{N \times M}$, which can be formulated as:

$$\begin{aligned}
 R_{n,m} &= \frac{\mathbf{A}_{n,m}}{\mathbf{A}_{n,m}^{spa}} = \frac{\sum_{m=1}^M \exp(\mathbf{S}_{n,m}) \cdot \widehat{M}_{n,m}}{\sum_{m=1}^M \exp(\mathbf{S}_{n,m})} \quad (9) \\
 &= \sum_{m \in \{m | \widehat{M}_{n,m} = 1\}} \mathbf{A}_{n,m}
 \end{aligned}$$

It can be seen that $R_{n,m} = R_{n,m'} = R_n, \forall m, m' \in \{1, \dots, M\}$, and thus it can be simplified as $\mathbf{R} \in \mathbb{R}^N$. Furthermore, R_n essentially represents the total weights of the critical tokens in the original full-attention. Considering the high cost of explicitly computing full attention, we implicitly estimate \mathbf{R} using pooled attention weights.

However, unlike video tokens, text tokens lack intra-block homogeneity; therefore, applying uniform pooling to them results in attention loss. Moreover, prior stud-

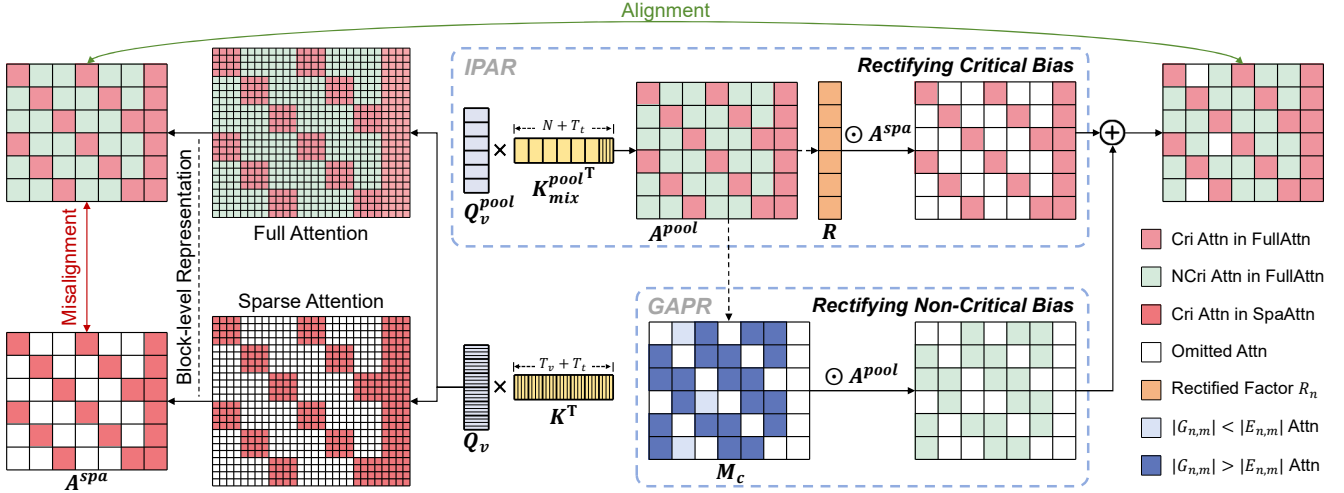


Figure 4. **Overview of Rectified SpaAttn.** Sparse attention is computed at the block level, exhibiting significant misalignment with full attention. IPAR isolates text tokens during pooling and reallocates pooled weights to obtain distribution-aligned implicit full attention, rectifying biases of critical blocks. GAPR estimates rectified gains and pooling errors to generate compensation mask, applying implicit attention compensation to non-critical blocks. The rectified sparse attention achieves strong alignment with the full attention.

ies [3, 34] have shown that text tokens occupy high attention weights in certain attention heads. Therefore, directly pooling disrupts the attention consistency, failing to accurately approximate the full-attention, as shown in Fig. 5.

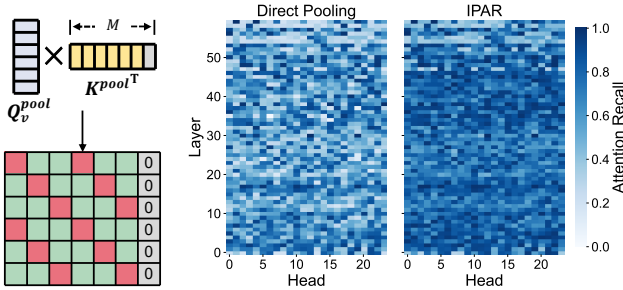


Figure 5. Left: Attention maps from direct pooling. Right: Attention recall of HunyuanVideo under 80% sparsity.

To address this issue, we propose **Isolated-Pooling Attention Reallocation (IPAR)**. Specifically, we isolate text tokens $K_t \in \mathbb{R}^{T_t \times d}$, and perform block-level pooling only on video tokens $K_v \in \mathbb{R}^{T_v \times d}$ to achieve $K_v^{pool} \in \mathbb{R}^{N \times d}$, yielding a mixed-granularity key sequence $K_{mix}^{pool} \in \mathbb{R}^{(N+T_t) \times d}$, on which the pooled attention weights $A_{mix}^{pool} \in \mathbb{R}^{N \times (N+T_t)}$ are computed:

$$A_{mix}^{pool} = \text{softmax}\left(\frac{Q_v^{pool} K_{mix}^{pool T}}{\sqrt{d}}\right) \quad (10)$$

where the attention weights for video and text tokens are denoted as $A_v^{pool} \in \mathbb{R}^{N \times N}$ and $A_t \in \mathbb{R}^{N \times T_t}$, respectively. Due to the different computation granularity between A_v^{pool} and A_t , block-level for the former and token-level for the latter, A_{mix}^{pool} exhibits an imbalance in cross-modal attention strength. To this end, we further propose a weight realloca-

tion strategy. We reweight the A_v^{pool} by block size B , ensuring that the weights of each block aligns with the token-level granularity. Then, we perform re-normalization:

$$\hat{A}_v^{pool} = \frac{A_v^{pool} \cdot B}{A_v^{pool} \cdot B + A_t}, \quad \hat{A}_t = \frac{A_t}{A_v^{pool} \cdot B + A_t} \quad (11)$$

Here, \hat{A}_v^{pool} and \hat{A}_t denote the token-level weights after re-allocation. We further aggregate \hat{A}_t by blocks to obtain the block-wise attention $\hat{A}_t^{pool} \in \mathbb{R}^{N \times \frac{T_t}{B}}$, and concatenate it with \hat{A}_v^{pool} to form the final implicit full attention $A^{pool} \in \mathbb{R}^{N \times M}$. IPAR produces cross-modally consistent pooled attention weights that accurately approximate full attention, thereby ensuring reliable computation of R_n to achieve rectified sparse attention $A_{n,m}^{spa'}$ of the critical tokens, as shown in Fig. 4.

$$R_n = \sum_{m \in \{m | \hat{M}_{n,m} = 1\}} A_{n,m}^{pool} \quad (12)$$

$$A_{n,m}^{spa'} = A_{n,m}^{spa} \cdot R_n \approx A_{n,m}$$

4.2. Rectifying the Bias of Non-Critical Tokens

In sparse attention, non-critical tokens are excluded from computation, losing their attention weights, as shown in Eq. 7. To rectify this bias, we compensate $A_{n,m}^{spa}$ using the pooled attention weights $A_{n,m}^{pool}$ aligning it with $A_{n,m}$. To evaluate $A_{n,m}^{pool} \approx A_{n,m}$ within the same granularity space, we remap the block-level weights $A_{n,m}^{pool} \in \mathbb{R}^1$ to the token-level weights $A_{n,m}^{pool} \in \mathbb{R}^{B^q \times B^k}$. Specifically, based on intra-block consistency, we replicate $A_{n,m}^{pool}$ along the query dimension to maintain shared weights within block, while uniformly distributing it along the key dimension to satisfy the softmax constraint, which can be formulated as:

$$A_{n,m}^{pool} = \frac{1}{B^k} (A_{n,m}^{pool} \otimes \mathbf{1}_{B^q \times B^k}) \quad (13)$$

Here, the Kronecker \otimes expands $A_{n,m}^{pool}$ into the token-level dimensions of $B^q \times B^k$.

However, the pooling operation only captures the overall block-level weights, failing to reflect the fine-grained variations among tokens within each block. Therefore, while pooling rectification introduces attention gains, it also incurs pooling errors, and the trade-off between the two leads to unstable rectification performance.

To address this issue, we propose **Gain-Aware Pooling Rectification (GAPR)**. Specifically, we theoretically estimate the attention gains and pooling errors at block level. GAPR performs rectification only when the estimated gain exceeds the error, thereby ensuring a stable performance improvement. The detailed implementation is as follows: **Attention Gain.** According to the analysis in Sec 3.2, the pooled attention weights exhibit high consistency with the full attention in both magnitude and distribution, providing a reasonable assumption for block-level gain modeling. Based on this, we define the attention gain $G \in \mathbb{R}^{N \times M}$ of non-critical blocks as the incremental change in attention weights before and after the rectification:

$$\begin{aligned} G_{n,m} &= A_{n,m}^{pool} - A_{n,m}^{spa} = \sum_{i \in B_n^q} \sum_{j \in B_m^k} |a_{i,j}^{pool}| \\ &= \sum_{i \in B_n^q} \sum_{j \in B_m^k} \text{softmax}(s_{i,j}^{pool}) \end{aligned} \quad (14)$$

Pooling Error. To estimate the bias introduced by the pooling approximation, we define the pooling error $E \in \mathbb{R}^{N \times M}$, which quantifies the discrepancy between the real attention weights and the pooled attention weights. For a non-critical block, the pooling error is formulated as:

$$\begin{aligned} E_{n,m} &= A_{n,m} - A_{n,m}^{pool} = \sum_{i \in B_n^q} \sum_{j \in B_m^k} |a_{i,j} - a_{i,j}^{pool}| \\ &\stackrel{(a)}{=} \sum_{i \in B_n^q} \sum_{j \in B_m^k} |\Delta a_{i,j}| = \sum_{i \in B_n^q} \sum_{j \in B_m^k} \text{softmax}(\Delta s_{i,j}) \end{aligned} \quad (15)$$

Here, (a) given that the softmax for the pooled and true weights are approximately equivalent, as proven in Appendix. $\Delta s_{i,j}$ can be efficiently computed as:

$$\begin{aligned} \Delta s_{i,j} &= \frac{q_i k_j^T - q_i^{pool} k_j^{pool T}}{\sqrt{d}} \\ &\stackrel{(b)}{=} \frac{(q_i - q_i^{pool}) k_j^{pool T} + q_i^{pool} (k_j - k_j^{pool})^T}{\sqrt{d}} \end{aligned} \quad (16)$$

where, (b) we omit higher-order error $\frac{(q_i - q_i^{pool})(k_j - k_j^{pool})^T}{\sqrt{d}}$.

Rectification. To ensure stable performance improvement, GAPR performs rectification only when the attention gains exceeds the pooling errors, i.e., $|G_{n,m}| > |E_{n,m}|$. As

shown in Fig. 4, this evaluation is performed at block level, producing a compensation mask $M_c \in \{0, 1\}^{N \times M}$, where $M_c = 1$ indicates that the corresponding block weights will be compensated by the implicit full attention:

$$A_{n,m}^{spa'} = A_{n,m}^{pool} \approx A_{n,m} \quad (17)$$

Here, $A_{n,m}^{spa'}$ denotes the rectified sparse attention of the non-critical tokens. Due to the monotonicity of the softmax function, we relax the rectification condition as:

$$\left| \sum_{i \in B_n^q} \sum_{j \in B_m^k} s_{i,j}^{pool} \right| > \left| \sum_{i \in B_n^q} \sum_{j \in B_m^k} \Delta s_{i,j} \right| \quad (18)$$

This eliminates the softmax, further improving efficiency.

Algorithm 1 Overall Process for Rectified SpaAttn

Require: Q, K, V , the number of video and text tokens T_v, T_t , *top-k*, weight threshold p , adjacency mask M_{adja}
Ensure: Attention output

- 1: Get video and text queries $Q_v, Q_t \leftarrow Q$
 - 2: Get video and text keys $K_v, K_t \leftarrow K$
 - 3: $Q_v^{pool}, K_v^{pool}, V^{pool} \leftarrow \text{Pooling}(Q_v), \text{Pooling}(K_v), \text{Pooling}(V)$, uniform pooling per block.
 - 4: **Implicit full-attention computation:**
 - 5: Mix keys: $K_{mix}^{pool} \leftarrow \text{Concat}(K_v^{pool}, K_t)$
 - 6: Mix weight: $A_{mix}^{pool} \leftarrow \text{softmax}\left(\frac{Q_v^{pool} K_{mix}^{pool T}}{\sqrt{d}}\right)$
 - 7: Pooled weight: $A^{pool} \leftarrow \text{Reallocate}(A_{mix}^{pool})$
 - 8: **Compensation mask generation:**
 - 9: Attention gain: $G \leftarrow G_{n,m} = \sum_{i,j \in B_n^q, B_m^k} s_{i,j}^{pool}$
 - 10: Pooling error: $E \leftarrow E_{n,m} = \sum_{i,j \in B_n^q, B_m^k} \Delta s_{i,j}$
 - 11: Compensation mask: $M_c \leftarrow |G| > |E|$
 - 12: **Sparse mask generation:**
 - 13: $M_I \leftarrow \text{top-k}(A^{pool}) \vee (\sum A^{pool} \odot M_I > p)$
 - 14: Sparse mask: $\widehat{M} \leftarrow M_I \vee M_{adja}$
 - 15: **Block-wise sparse attention:**
 - 16: Output: $O_v \leftarrow \text{SparseKernel}(Q_v, K, V, \widehat{M})$
 - 17: Text output: $O_t \leftarrow \text{FullKernel}(Q_t, K, V)$
 - 18: **Attention bias rectification:**
 - 19: Rectified factor: $R \leftarrow R_n = \sum_{m=1}^M A_{n,m}^{pool} \cdot \widehat{M}_{n,m}$
 - 20: Rect cri: $O_v^{cri} \leftarrow O_v \odot R$
 - 21: Rect ncri: $O_v^{ncri} \leftarrow A^{pool} \odot (-\widehat{M} \wedge M_c) \cdot V^{pool}$
 - 22: Rectified output: $O'_v \leftarrow O_v^{cri} + O_v^{ncri}$
 - 23: **Return** $\text{Concat}(O'_v, O_t)$
-

4.3. Implementation and Modularization

Rectified SpaAttn implements dynamic attention sparsity in three steps: ① implicit full-attention computation with mask generation, ② block-wise sparse attention, and ③ attention bias rectification. Alg. 1 shows the overall process.

- IAPR pools multimodal tokens to compute pooled attention weights, which serve as the implicit full attention

Table 1. Quality and efficiency results on HunyuanVideo-T2V (50 steps, 128 frames, 720p videos).

Method	VR \uparrow	I.Q. \uparrow	A.Q. \uparrow	S.C. \uparrow	M.S. \uparrow	B.C. \uparrow	VBench \uparrow	Sparsity	FLOPs	Latency (s)	Speedup
HunyuanVideo	0.0986	67.31	56.20	96.33	99.31	96.65	83.16	0%	612.38 PFLOPs	2425	1.00 \times
SVG	0.0890	64.01	55.84	94.64	99.35	95.88	81.94	78.91%	320.38 PFLOPs	1010	2.43 \times
SVG2	0.0906	64.30	54.97	94.45	99.35	95.73	81.76	79.26%	314.27 PFLOPs	986	2.46 \times
GRAT-R	0.0752	65.12	56.11	93.84	99.23	95.96	82.05	86.14%	289.39 PFLOPs	830	2.92 \times
RadialAttention	0.0819	62.80	59.17	93.54	99.31	95.79	82.12	78.25%	323.75 PFLOPs	973	2.49 \times
Jenga	0.0855	66.39	55.74	95.01	99.12	95.90	82.43	74.64%	335.38 PFLOPs	1050	2.31 \times
Ours	0.0965	65.99	56.30	96.82	99.37	97.19	83.13	79.68%	310.27 PFLOPs	970	2.50 \times
Ours	0.0890	64.32	55.92	96.10	99.42	97.08	82.57	88.95%	278.11 PFLOPs	729	3.33 \times
Ours+Tea	0.0883	64.61	55.61	96.39	99.33	96.73	82.53	78.36%	180.91 PFLOPs	463	5.24\times

to assess block importance and guide bias rectification. GAPR evaluates attention gains and pooling errors for non-critical blocks, activating compensation mask. For sparse mask generation, similar to Jenga [34], we select the *top-k* important blocks with weights above a threshold p , while retaining spatial-temporal neighbors blocks.

- We build sparse attention on FlashAttention2 with Triton, enabling efficient block-wise computation driven by the sparse mask. Meanwhile, other attention computations remain block-wise to further improve efficiency.
- Bias rectification is applied to the sparse attention results. For critical tokens, weighted correction is performed using rectification factors derived from the implicit full attention. For non-critical tokens, attention information is recovered via the compensation mask by combining the implicit full attention with pooled values.

Since all rectification are built on pooled vectors, the additional overhead is negligible. To improve usability and transferability, Rectified SpaAttn is encapsulated as a plug-and-play module, enabling seamless integration into other DiT models with minimal code, as shown in Fig. 6.

```

from rectified_sparse import rectified_sparse_attention
# params: {top_k, p, M_adja} - sparse parameters
q, k, v = project_qkv(hidden_states, qkv_weights)
-out = original_attention(q, k, v)
+out = rectified_sparse_attention(q, k, v, params)
return out

```

Figure 6. Minimal Integration of Rectified SpaAttn.

5. Experiment

Models. We evaluate Rectified SpaAttn on open-sourced video generation models including HunyuanVideo-T2V-13B [10] and Wan2.1-I2V/T2V-14B [25]. We further extend it to image generation model Flux.1-dev-12B [11].

Metrics. We use *Vision Reward* (VR) [31], and VBench [7] key metrics to evaluate video quality, including *imaging quality* (I.Q.), *aesthetic quality* (A.Q.), *subject consistency* (S.C.), *motion smoothness* (M.S.), and *background consistency* (B.C.). Their average is reported as VBench. We evaluate image quality using *Image Reward* (IR \uparrow) [30], *FID* \downarrow [6], *CLIP* \uparrow [21], *SSIM* \uparrow , *PSNR* \uparrow , and *LPIPS* \downarrow . The efficiency of the sparsity mechanism is quantified by the

Table 2. Generation results on Flux.1-dev (50 steps, 4K images).

Method	IR	FID	CLIP	SSIM	PSNR	LPIPS	Sparsity	Speedup
Flux.1-dev	1.0760	-	26.50	-	-	-	0%	1.00 \times
GRAT-R	0.8415	15.59	26.34	0.734	19.58	0.283	96.20%	1.27 \times
Jenga	0.9562	12.31	26.35	0.953	32.10	0.032	73.86%	1.32 \times
Ours	1.0131	5.37	26.43	0.976	36.89	0.015	74.05%	1.40 \times
Ours	1.0050	10.15	26.48	0.965	33.26	0.029	87.66%	1.60 \times
Ours+Tea	1.0047	10.23	26.47	0.964	33.26	0.029	87.66%	4.15\times

Sparsity, defined as the computations removed relative to full attention. To intuitively evaluate the end-to-end efficiency, we further measure *FLOPs*, *Latency*, and *Speedup*.

Datasets. We use prompts in Penguin Benchmark [10] for text-to-video generation, using prompt-image pairs from VBench [7] and cropping images to match 720p resolution for image-to-video generation, and using the same COCO prompts as GRAT [22] for text-to-image generation.

Baselines. We compare Rectified SpaAttn with state-of-the-art sparse methods including SVG [27], SVG2 [32], GRAT-R [22], RadialAttention [12], and Jenga [34]. To ensure a fair comparison, we match their efficiency to ours by tuning the sparsity ratio, as detailed in the Appendix.

Implementation Details. We implement Rectified SpaAttn as a plug-and-play module with customized kernels based on FlashAttention [4], and benchmark it on an NVIDIA H100 PCIe with CUDA 12.4. Rectified SpaAttn introduces no empirical parameters, allowing users to flexibly balance efficiency and quality by adjusting the sparsity ratio. Details of the experimental setup are provided in the Appendix. For Wan2.1-T2V, we retain a 5-step warm-up following prior work [12, 32]. We further integrate it with the caching method TeaCache [14] to achieve a higher speedup.

5.1. Quality and Efficiency Evaluation

As reported in Tab. 1, 2, and 3, at comparable sparsity, Rectified SpaAttn consistently outperforms all baselines while achieving higher speedups. As the sparsity increases, Rectified SpaAttn not only pushes the limits of sparse speedup but also maintains high quality. Moreover, it can be seamlessly combined with caching techniques to further boost inference efficiency. Specifically, Rectified SpaAttn achieves VR scores of 0.1026 and 0.1391 on Wan2.1-T2V and Wan2.1-I2V, respectively, at approximately 75% sparsity. On HunyuanVideo, it attains a 3.33 \times speedup at 88.95% sparsity while achieving a VBench Score of 82.57. By com-

Table 3. Quality and efficiency results on Wan2.1-T2V / I2V (50 steps, 81 frames, 720p videos).

Method	VR \uparrow	I.Q. \uparrow	A.Q. \uparrow	S.C. \uparrow	M.S. \uparrow	B.C. \uparrow	VBench \uparrow	Sparsity	FLOPs	Latency (s)	Speedup
Wan2.1-T2V	0.1029	68.82	60.56	96.24	98.68	96.43	84.15	0%	658.46 PFLOPs	2731	1.00 \times
SVG	0.0863	65.24	60.66	95.84	98.74	96.28	83.35	75.90%	413.11 PFLOPs	1631	1.67 \times
SVG2	0.0979	65.58	60.09	96.32	99.04	96.32	83.47	75.57%	416.57 PFLOPs	1643	1.66 \times
RadialAttention	0.0977	65.09	60.05	96.29	99.19	96.72	83.46	75.91%	414.25 PFLOPs	1634	1.67 \times
Jenga	0.1005	65.46	60.14	95.96	98.85	96.42	83.37	73.69%	419.88 PFLOPs	1656	1.65 \times
Ours	0.1026	65.67	59.78	96.91	99.21	97.01	83.72	74.88%	415.34 PFLOPs	1624	1.68 \times
Ours	0.0991	65.40	58.94	96.87	99.20	96.92	83.47	79.71%	398.75 PFLOPs	1515	1.80 \times
Ours+Tea	0.0903	63.68	58.86	97.03	99.18	97.08	83.17	74.82%	173.46 PFLOPs	592	4.61\times
Wan2.1-I2V	0.1405	71.41	60.39	93.14	98.02	94.68	83.53	0%	645.45 PFLOPs	2754	1.00 \times
SVG	0.1156	71.07	59.23	91.99	97.94	93.73	82.79	69.27%	428.75 PFLOPs	1794	1.54 \times
SVG2	0.1256	71.54	59.93	92.96	97.97	94.38	83.35	70.11%	425.64 PFLOPs	1763	1.56 \times
Jenga	0.1142	70.02	57.90	90.88	97.86	92.92	81.92	73.68%	385.27 PFLOPs	1543	1.78 \times
Ours	0.1391	71.79	60.65	93.70	98.48	94.84	83.89	74.69%	375.17 PFLOPs	1522	1.81 \times
Ours	0.1288	71.09	59.71	93.29	98.53	94.52	83.43	83.91%	348.56 PFLOPs	1327	2.08 \times
Ours+Tea	0.1195	70.85	59.62	94.34	99.03	95.51	83.87	74.64%	91.34 PFLOPs	307	8.97\times

Table 4. Ablation study of IPAR and GAPR on HunyuanVideo.

Method			VR \uparrow	VBench \uparrow	Latency	Speedup
Rectify	IPAR	GAPR				
\times	\times	\times	0.0585	81.15	719 s	3.37 \times
\checkmark	\times	\times	0.0435	79.85	725 s	3.34 \times
\checkmark	\checkmark	\times	0.0805	81.92	726 s	3.34 \times
\checkmark	\checkmark	\checkmark	0.0890	82.57	729 s	3.33 \times

binning with TeaCache, our method achieves 5.24 \times , 8.97 \times , and 4.15 \times speedups on HunyuanVideo-T2V, Wan2.1-I2V, and Flux.1-dev, respectively.

5.2. Ablation Study

Effectiveness and Efficiency of IPAR and GAPR. We use Jenga with 88.95% sparsity as the baseline. As shown in Tab. 4, under high sparsity, Jenga’s performance degrades significantly, with the VR score dropping to 0.0585. When rectification is applied using directly pooled attention map, performance further degrades, indicating its poor alignment with full attention, leading to misleading rectifications. By introducing IPAR, the performance improves significantly, indicating that IPAR effectively captures distribution-aligned implicit full attention, thereby rectifying the bias of critical tokens. GAPR effectively constrains the rectification of non-critical tokens to ensure the gains surpass pooling errors, thereby achieving stable performance improvements. Moreover, they incur negligible overhead with minimal impact on inference efficiency.

Implicit Full Attention Alignment. Alignment between the implicit and the full attention serves as the foundation for effective rectification. We evaluate this alignment both numerically and distributionally using normalized L1 error and cosine similarity, respectively. As shown in Fig. 7, compared with directly pooled attention weights (DP), the implicit full attention obtained by IPAR exhibits higher consistency with the true full attention, demonstrating its effectiveness in attention alignment.

Advantages of Gain-Aware Rectification. We validate the effectiveness of GAPR across different models and sparsity

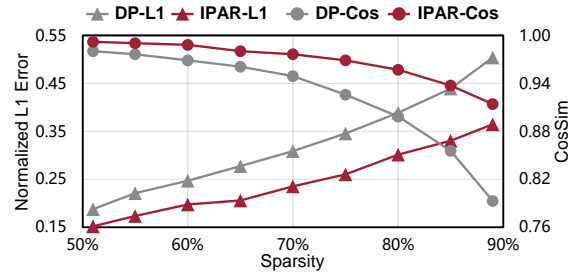


Figure 7. Alignment evaluation of IPAR on HunyuanVideo.

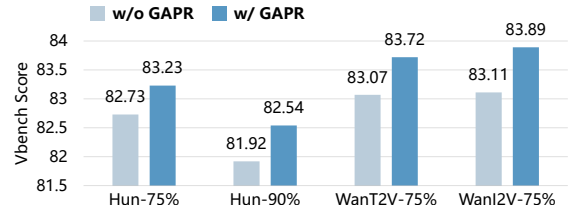


Figure 8. Effectiveness evaluation of GAPR.

levels. As shown in Fig. 8, GAPR consistently and significantly improves the performance of sparse models.

6. Conclusion

In this paper, we revisit attention sparsity and propose a new paradigm that improves sparse attention accuracy through bias rectification. Building on this, we propose Rectified SpaAttn, which rectifies attention allocation biases with implicit full attention reference, thereby enhancing the alignment between sparse and full attention maps. By the isolated-pooling attention reallocation, Rectified SpaAttn derives a distribution-aligned implicit full attention, effectively rectifying the attention bias of critical tokens. By the gain-aware pooling rectification, Rectified SpaAttn ensures that the rectified gains consistently surpass the pooling errors, effectively rectifying the attention bias of non-critical tokens. Extensive experiments show that Rectified SpaAttn achieves superior generation quality even under high sparsity, making video generation more efficient and practical.

References

- [1] Pierre Blanchard, Desmond J Higham, and Nicholas J Higham. Accurately computing the log-sum-exp and softmax functions. *IMA Journal of Numerical Analysis*, 41(4): 2311–2330, 2021. [1](#)
- [2] Thibault Castells, Hyoung-Kyu Song, Bo-Kyeong Kim, and Shinkook Choi. Ld-pruner: Efficient pruning of latent diffusion models using task-agnostic insights. In *Proceedings of the IEEE/CVF Conference on Computer Vision and Pattern Recognition*, pages 821–830, 2024. [3](#)
- [3] Pengtao Chen, Xianfang Zeng, Maosen Zhao, Peng Ye, Mingzhu Shen, Wei Cheng, Gang Yu, and Tao Chen. Sparse-vdit: Unleashing the power of sparse attention to accelerate video diffusion transformers. *arXiv preprint arXiv:2506.03065*, 2025. [5](#)
- [4] Tri Dao. Flashattention-2: Faster attention with better parallelism and work partitioning. *arXiv preprint arXiv:2307.08691*, 2023. [2](#), [3](#), [7](#)
- [5] Zhengyang Geng, Mingyang Deng, Xingjian Bai, J Zico Kolter, and Kaiming He. Mean flows for one-step generative modeling. *arXiv preprint arXiv:2505.13447*, 2025. [3](#)
- [6] Martin Heusel, Hubert Ramsauer, Thomas Unterthiner, Bernhard Nessler, and Sepp Hochreiter. Gans trained by a two time-scale update rule converge to a local nash equilibrium. *Advances in neural information processing systems*, 30, 2017. [7](#)
- [7] Ziqi Huang, Yanan He, Jiashuo Yu, Fan Zhang, Chenyang Si, Yuming Jiang, Yuanhan Zhang, Tianxing Wu, Qingyang Jin, Nattapol Chanpaisit, et al. Vbench: Comprehensive benchmark suite for video generative models. In *Proceedings of the IEEE/CVF Conference on Computer Vision and Pattern Recognition*, pages 21807–21818, 2024. [2](#), [7](#)
- [8] Huiqiang Jiang, Yucheng Li, Chengruidong Zhang, Qianhui Wu, Xufang Luo, Surin Ahn, Zhenhua Han, Amir H Abdi, Dongsheng Li, Chin-Yew Lin, et al. Minference 1.0: Accelerating pre-filling for long-context llms via dynamic sparse attention. *Advances in Neural Information Processing Systems*, 37:52481–52515, 2024. [3](#), [4](#)
- [9] Armand Joulin, Moustapha Cissé, David Grangier, Hervé Jégou, et al. Efficient softmax approximation for gpus. In *International conference on machine learning*, pages 1302–1310. PMLR, 2017. [1](#)
- [10] Weijie Kong, Qi Tian, Zijian Zhang, Rox Min, Zuozhuo Dai, Jin Zhou, Jiangfeng Xiong, Xin Li, Bo Wu, Jianwei Zhang, et al. Hunyuanvideo: A systematic framework for large video generative models. *arXiv preprint arXiv:2412.03603*, 2024. [1](#), [2](#), [3](#), [7](#)
- [11] Black Forest Labs. Flux: Official inference repository for flux.1 models. <https://github.com/black-forest-labs/flux>, 2024. Accessed: 2024-11-12. [2](#), [7](#)
- [12] Xingyang Li, Muiyang Li, Tianle Cai, Haocheng Xi, Shuo Yang, Yujun Lin, Lvmin Zhang, Songlin Yang, Jinbo Hu, Kelly Peng, et al. Radial attention: Sparse attention with energy decay for long video generation. *arXiv preprint arXiv:2506.19852*, 2025. [2](#), [3](#), [7](#), [1](#)
- [13] Zhikai Li, Xuewen Liu, Dongrong Joe Fu, Jianquan Li, Qingyi Gu, Kurt Keutzer, and Zhen Dong. K-sort arena: Efficient and reliable benchmarking for generative models via k-wise human preferences. In *Proceedings of the Computer Vision and Pattern Recognition Conference*, pages 9131–9141, 2025. [3](#)
- [14] Feng Liu, Shiwei Zhang, Xiaofeng Wang, Yujie Wei, Haonan Qiu, Yuzhong Zhao, Yingya Zhang, Qixiang Ye, and Fang Wan. Timestep embedding tells: It’s time to cache for video diffusion model. In *Proceedings of the Computer Vision and Pattern Recognition Conference*, pages 7353–7363, 2025. [2](#), [3](#), [7](#)
- [15] Xuewen Liu, Zhikai Li, Junrui Xiao, and Qingyi Gu. Eda-dm: Enhanced distribution alignment for post-training quantization of diffusion models. *arXiv preprint arXiv:2401.04585*, 2024. [3](#)
- [16] Xuewen Liu, Zhikai Li, and Qingyi Gu. Cachequant: Comprehensively accelerated diffusion models. In *Proceedings of the Computer Vision and Pattern Recognition Conference*, pages 23269–23280, 2025. [3](#)
- [17] Xuewen Liu, Zhikai Li, Minghao Jiang, Mengjuan Chen, Jianquan Li, and Qingyi Gu. Dilatequant: Accurate and efficient quantization-aware training for diffusion models via weight dilation. In *Proceedings of the 33rd ACM International Conference on Multimedia*, pages 8399–8408, 2025. [3](#)
- [18] Xinyin Ma, Gongfan Fang, and Xinchao Wang. Deepcache: Accelerating diffusion models for free. In *Proceedings of the IEEE/CVF conference on computer vision and pattern recognition*, pages 15762–15772, 2024. [3](#)
- [19] Chenlin Meng, Robin Rombach, Ruiqi Gao, Diederik Kingma, Stefano Ermon, Jonathan Ho, and Tim Salimans. On distillation of guided diffusion models. In *Proceedings of the IEEE/CVF conference on computer vision and pattern recognition*, pages 14297–14306, 2023. [3](#)
- [20] William Peebles and Saining Xie. Scalable diffusion models with transformers. In *Proceedings of the IEEE/CVF international conference on computer vision*, pages 4195–4205, 2023. [1](#)
- [21] Alec Radford, Jong Wook Kim, Chris Hallacy, Aditya Ramesh, Gabriel Goh, Sandhini Agarwal, Girish Sastry, Amanda Askell, Pamela Mishkin, Jack Clark, et al. Learning transferable visual models from natural language supervision. In *International conference on machine learning*, pages 8748–8763. PmlR, 2021. [7](#)
- [22] Sucheng Ren, Qihang Yu, Ju He, Alan Yuille, and Liang-Chieh Chen. Grouping first, attending smartly: Training-free acceleration for diffusion transformers. *arXiv preprint arXiv:2505.14687*, 2025. [2](#), [3](#), [7](#), [1](#)
- [23] Jiaming Tang, Yilong Zhao, Kan Zhu, Guangxuan Xiao, Baris Kasikci, and Song Han. Quest: Query-aware sparsity for efficient long-context llm inference. *arXiv preprint arXiv:2406.10774*, 2024. [2](#), [3](#)
- [24] Ashish Vaswani, Noam Shazeer, Niki Parmar, Jakob Uszkoreit, Llion Jones, Aidan N Gomez, Łukasz Kaiser, and Illia Polosukhin. Attention is all you need. *Advances in neural information processing systems*, 30, 2017. [1](#)

- [25] Team Wan, Ang Wang, Baole Ai, Bin Wen, Chaojie Mao, Chen-Wei Xie, Di Chen, Feiwu Yu, Haiming Zhao, Jianxiao Yang, et al. Wan: Open and advanced large-scale video generative models. *arXiv preprint arXiv:2503.20314*, 2025. [1](#), [2](#), [7](#)
- [26] Dennis Wei, Haoze Wu, Min Wu, Pin-Yu Chen, Clark Barrett, and Eitan Farchi. Convex bounds on the softmax function with applications to robustness verification. In *International Conference on Artificial Intelligence and Statistics*, pages 6853–6878. PMLR, 2023. [1](#)
- [27] Haocheng Xi, Shuo Yang, Yilong Zhao, Chenfeng Xu, Muyang Li, Xiuyu Li, Yujun Lin, Han Cai, Jintao Zhang, Dacheng Li, et al. Sparse videogen: Accelerating video diffusion transformers with spatial-temporal sparsity. *arXiv preprint arXiv:2502.01776*, 2025. [2](#), [3](#), [7](#), [1](#)
- [28] Yifei Xia, Suhan Ling, Fangcheng Fu, Yujie Wang, Huixia Li, Xuefeng Xiao, and Bin Cui. Training-free and adaptive sparse attention for efficient long video generation. *arXiv preprint arXiv:2502.21079*, 2025. [2](#), [3](#)
- [29] Guangxuan Xiao, Yuandong Tian, Beidi Chen, Song Han, and Mike Lewis. Efficient streaming language models with attention sinks, 2024. URL <https://arxiv.org/abs/2309.17453>, 1, 2024. [2](#), [3](#)
- [30] Jiazheng Xu, Xiao Liu, Yuchen Wu, Yuxuan Tong, Qinkai Li, Ming Ding, Jie Tang, and Yuxiao Dong. Imagereward: Learning and evaluating human preferences for text-to-image generation. *Advances in Neural Information Processing Systems*, 36:15903–15935, 2023. [7](#)
- [31] Jiazheng Xu, Yu Huang, Jiale Cheng, Yuanming Yang, Jiajun Xu, Yuan Wang, Wenbo Duan, Shen Yang, Qunlin Jin, Shurun Li, et al. Visionreward: Fine-grained multi-dimensional human preference learning for image and video generation. *arXiv preprint arXiv:2412.21059*, 2024. [2](#), [7](#)
- [32] Shuo Yang, Haocheng Xi, Yilong Zhao, Muyang Li, Jintao Zhang, Han Cai, Yujun Lin, Xiuyu Li, Chenfeng Xu, Kelly Peng, et al. Sparse videogen2: Accelerate video generation with sparse attention via semantic-aware permutation. *arXiv preprint arXiv:2505.18875*, 2025. [2](#), [3](#), [7](#), [1](#)
- [33] Peiyuan Zhang, Yongqi Chen, Runlong Su, Hangliang Ding, Ion Stoica, Zhengzhong Liu, and Hao Zhang. Fast video generation with sliding tile attention. *arXiv preprint arXiv:2502.04507*, 2025. [2](#), [3](#)
- [34] Yuechen Zhang, Jinbo Xing, Bin Xia, Shaoteng Liu, Bohao Peng, Xin Tao, Pengfei Wan, Eric Lo, and Jiaya Jia. Training-free efficient video generation via dynamic token carving. *arXiv preprint arXiv:2505.16864*, 2025. [2](#), [3](#), [4](#), [5](#), [7](#), [1](#)
- [35] Zhenyu Zhang, Ying Sheng, Tianyi Zhou, Tianlong Chen, Lianmin Zheng, Ruisi Cai, Zhao Song, Yuandong Tian, Christopher Ré, Clark Barrett, et al. H2o: Heavy-hitter oracle for efficient generative inference of large language models. *Advances in Neural Information Processing Systems*, 36:34661–34710, 2023. [3](#)

Rectified SpaAttn: Revisiting Attention Sparsity for Efficient Video Generation

Supplementary Material

7. Proof: Equivalence Analysis of Softmax Normalization under Pooling for DiTs

In this section, we show that the pooled attention weights of DiT visual tokens share approximately equivalent softmax normalization denominators with the true attention weights, allowing the $\Delta w_{i,j} = w_{i,j} - w_{i,j}^{pool}$. The proof proceeds as follows.

For query q_i , the softmax denominator of $w_{i,j}$ is expressed as:

$$\begin{aligned} S_{sum}(i) &= \sum_{m=1}^M \sum_{j \in B_m^k} \exp\left(\frac{q_i k_j^T}{\sqrt{D}}\right) \\ &= \sum_{m=1}^M \sum_{j \in B_m^k} \exp(s_{i,j}) \end{aligned} \quad (19)$$

The softmax denominator of $w_{i,j}^{pool}$ is expressed as:

$$\begin{aligned} S_{sum}^{pool}(i) &= \sum_{m=1}^M \sum_{j \in B_m^k} \exp\left(\frac{q_i^{pool} k_j^{poolT}}{\sqrt{D}}\right) \\ &= \sum_{m=1}^M \sum_{j \in B_m^k} \exp(s_{i,j}^{pool}) \end{aligned} \quad (20)$$

For q_i interacting with the m -th key block K_m , the average intra-block attention score $s_{i,m}$ is given by:

$$s_{i,m} = \frac{1}{B^k} \sum_{j \in B_m^k} s_{i,j} = \frac{q_i k_j^{poolT}}{\sqrt{D}} \quad (21)$$

The softmax denominator of $w_{i,j}$ within this block is:

$$\begin{aligned} S_m(i) &= \sum_{j \in B_m^k} \exp(s_{i,j}) \\ &= B^k \cdot \exp(s_{i,m}) \cdot \frac{1}{B^k} \sum_{j \in B_m^k} \exp(s_{i,j} - s_{i,m}) \\ &= B^k \cdot \exp(s_{i,m}) \cdot A_{i,m} \end{aligned} \quad (22)$$

We define:

$$A_{i,m} = \frac{1}{B^k} \sum_{j \in B_m^k} \exp(s_{i,j} - s_{i,m}) = \mathbb{E}[\exp(\varepsilon_{i,j})] \quad (23)$$

where $\varepsilon_{i,j} = s_{i,j} - s_{i,m}$ denotes the zero-mean intra-block deviation of the attention scores. Applying a second-order

Taylor expansion to the exponential function with respect to ε :

$$\exp(\varepsilon_{i,j}) = 1 + \varepsilon + \frac{1}{2}\varepsilon^2 + O(\varepsilon^3) \quad (24)$$

Given the randomness of the pooling error, $\mathbb{E}[\varepsilon_{i,j}] = 0$, and omitting higher-order terms, $A_{i,m}$ simplifies to:

$$A_{i,m} = 1 + \frac{1}{2}\varepsilon^2 \quad (25)$$

Here, ε^2 essentially corresponds to the variance of the true intra-block attention scores. Substituting Eq. 22 and Eq. 25 into Eq. 19 yields:

$$S_{sum}(i) = \sum_{m=1}^M B^k \cdot \exp(s_{i,m}) \cdot \left(1 + \frac{1}{2}\varepsilon^2\right) \quad (26)$$

Previous studies [1, 9, 26] have shown that introducing small perturbations during softmax computation does not affect its validity. We define the condition $|S_{sum} - S_{sum}^{pool}| < 5\%|S_{sum}|$ as a criterion for introducing small perturbations. Based on Eq. 20 and Eq. 26, this condition is evaluated across all layers of the HunyuanVideo in a block-wise manner. Experimental statistics show that 99.3% of block interactions satisfy this criterion, thereby demonstrating the approximate equivalence of the softmax normalization denominators between the true and pooled attention weights.

8. Implementations

Baselines. We compare our method with state-of-the-art baselines including SVG [27], SVG2 [32], GRAT [22], RadialAttention [12], and Jenga [34]. We evaluate performance by directly using the official open-source implementations. For a fair comparison, we tune their sparsity parameters to match the efficiency of our method. For SVG2, simply adjusting the sparsity ratio leads to performance degradation; therefore, we appropriately modify its warmup schedule.

SVG: For HunyuanVideo, Wan2.1-T2V, and Wan2.1-I2V, we set the sparsity parameters *sparsity* to 0.15, 0.25, and 0.2, respectively.

SVG2: For HunyuanVideo, Wan2.1T2V, and Wan2.1I2V, we set the sparsity parameters *top-p.k* parameters to 0.6, 0.7, and 0.75, respectively. In addition, the 10-step warmup for HunyuanVideo is reduced to 5 steps.

GRAT: For HunyuanVideo and Flux.1-dev, we employ local attention windows over surrounding blocks, controlling the window size to 5 in both 3D and 2D attention spaces.

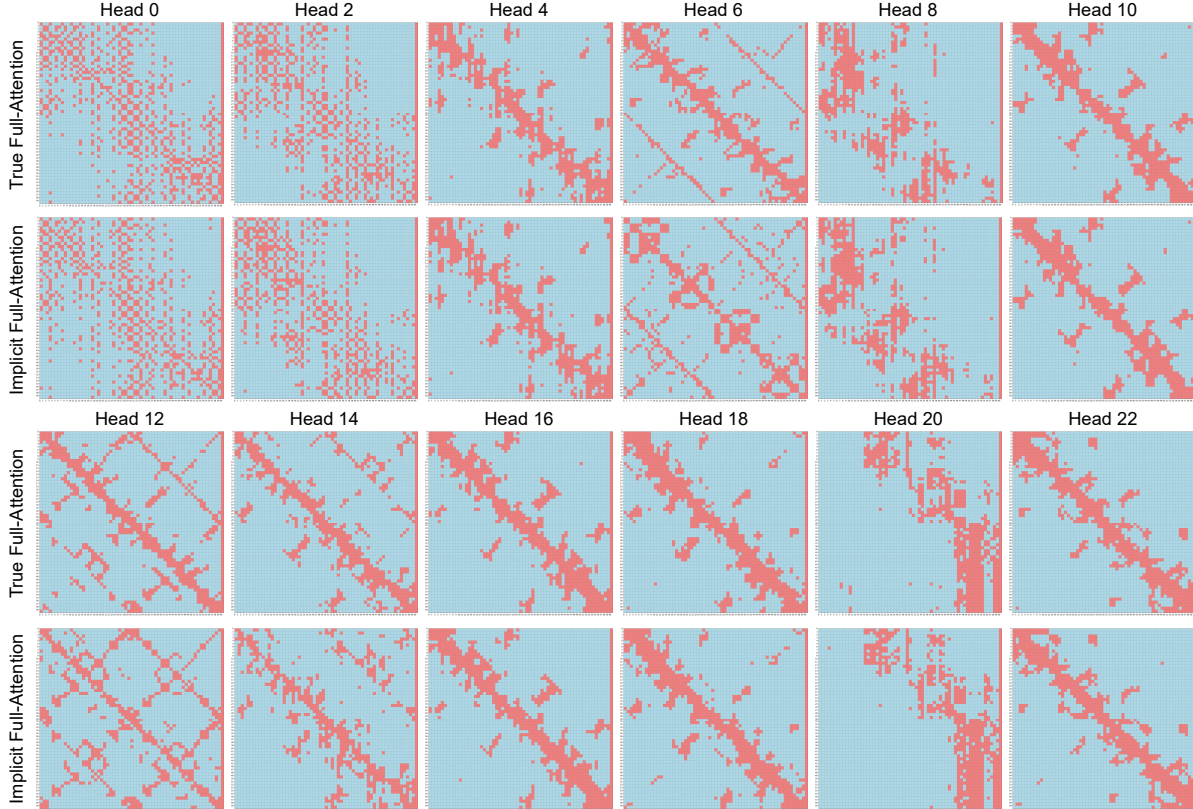


Figure 9. Implicit and truth full-attention maps of the first attention layer in HunyuanVideo under a 7,680 token sequence.

RadialAttention: For HunyuanVideo and Wan2.1-T2V, we set the *decay* parameters to 0.6 and 0.2, respectively.

Jenga: For HunyuanVideo, we set the sparsity parameters *top.k* to 0.75 and *p* to 0.3; for Wan2.1-T2V and Wan2.1-I2V, we set *top.k* to 0.8 and *p* to 0.8; for Flux.1-dev, we set *top.k* to 0.5 and *p* to 0.5.

Rectified SpaAttn. Our method involves two parameters for controlling sparsity ratio. *top.k* determines the number of important blocks to retain, while *p* sets the threshold such that the sum of attention weights of the retained blocks exceeds this value. Prior to inference, we reorder the token sequence using a Space-Filling Curve [34] to enhance intra-block consistency. Except for retaining a 5-step warmup for Wan2.1-T2V, no warmup is applied to other models. When combined with Teacache [14], we preserve its existing cache architecture and do not modify any cache parameters. The settings for the main experimental results are summarized in Table 5. The table colors are aligned with those used in the main results.

9. Visualization of Generation Results

We provide the videos and images generated by Rectified SpaAttn on our open-source repository at <https://github.com/BienLuky/Rectified-SpaAttn>.

Table 5. Detailed parameters of the main results.

Model	Settings	<i>top-k</i>	<i>p</i>	<i>tea-thresh</i>
HunyuanVideo	Ours	0.2	0.3	-
	Ours	0.1	0.3	-
	Ours+Tea	0.2	0.3	0.15
Wan2.1-T2V	Ours	0.25	0.3	-
	Ours	0.2	0.3	-
	Ours+Tea	0.25	0.3	0.2
Wan2.1-I2V	Ours	0.25	0.3	-
	Ours	0.15	0.3	-
	Ours+Tea	0.25	0.3	0.3
Flux.1-dev	Ours	0.25	0.3	-
	Ours	0.1	0.3	-
	Ours+Tea	0.1	0.3	0.8

10. Visualization of Implicit Full-Attention Maps

In this section, we visualize the implicit full-attention maps obtained by IPAR. As shown in Fig. 9, our implicit full-attention exhibits a high degree of distributional alignment with the truth full attention, providing a solid foundation for the effectiveness of our rectification mechanism.